

Future changes in intense tropical cyclone hazards in the Pearl River Delta region: An air-wave-ocean coupled model study

Zhenning Li

zhenningli91@gmail.com

The Hong Kong University of Science and Technology <https://orcid.org/0000-0002-7770-6867>

Jimmy C.H. Fung

The Hong Kong University of Science and Technology

Mau Fung Wong

The Hong Kong University of Science and Technology

Shangfei Lin

The Hong Kong University of Science and Technology

Fenyng Cai

Potsdam Institute for Climate Impact Research (PIK) e V: Potsdam-Institut für Klimafolgenforschung (PIK) e V

Wenfeng Lai

The Hong Kong University of Science and Technology

Alexis K.H. Lau

The Hong Kong University of Science and Technology

Research Article

Keywords:

Posted Date: November 29th, 2023

DOI: <https://doi.org/10.21203/rs.3.rs-3625663/v1>

License:  This work is licensed under a Creative Commons Attribution 4.0 International License.

[Read Full License](#)

Version of Record: A version of this preprint was published at Natural Hazards on March 9th, 2024. See the published version at <https://doi.org/10.1007/s11069-024-06510-7>.

Abstract

The Pearl River Delta (PRD) region is highly vulnerable to tropical cyclone (TC)-caused coastal hazards due to its long and meandering shoreline and well-developed economy. With global warming expected to continue or worsen in the rest of the 21st century, this study examines the TC impact on the PRD coastal regions by reproducing three intense landfalling TCs using a sophisticated air-wave-ocean coupled model of high spatial resolution (1-km atmosphere and 500-m wave and ocean). The simulations are conducted using present-day reanalysis data and the same TCs occurring in a pseudo-global warming scenario projected for the 2090s. Results indicate that the coupled model accurately reproduces the air-wave-ocean status during the TC episodes. The 2090s thermodynamic status effectively increases the intensity of intense TCs, leading to more severe coastal hazards including gale, rainstorm, and storm surges and waves. On average, the maximum surface wind speed within 50–200 km to the right of the TC center can increase by 4.3 m/s (+ 22%). The 99th and the 99.9th percentile of accumulated rainfall will increase from 405 mm to 475 mm (+ 17.3%), and from 619 mm to 735 mm (+ 18.6%), respectively. The maximum significant wave height at the ocean is lifted by an average of 57 cm (+ 13.8%), and the coastline typically faces a 40–80 cm increase. The maximum storm surges are lifted by 30–80 cm over the open sea but aggravate much higher along the coastline, especially for narrowing estuaries. For Typhoon Vicente (2012), there is more than a 200 cm wave height increase observed both at open sea and along the coastline. In the 2090s context, a combination of mean sea level rise, storm surge, and wave height can reach more than 300 cm increase in total water level at certain hot-spot coastlines, without considering the superposition of spring tides.

Introduction

Landfalling tropical cyclones (TCs) are intense weather systems that can cause a range of coastal hazards, including storm surges and waves, coastal erosion, wind induced damage, rainstorms, and secondary hazards like landslides and inland flooding (Tran et al. 2022, Wu et al. 2022). The impact of landfalling TCs can vary depending on the severity and location of the storm, as well as the vulnerability of the affected communities (Wang et al. 2008, Knutson et al. 2010, Knutson et al. 2019, Chu et al. 2020). The Pearl River Delta (PRD) region, with its long and meandering coastline and well-developed economy, is highly vulnerable to TC-caused coastal disasters (Chan 2008, Chen et al. 2020). Recent TCs, such as Typhoon Hato (2017) and Mangkhut (2018), have demonstrated the devastating impact these storms can have, causing widespread damage and losses (Liu and Chan 2020). The estimated direct economic loss due to Mangkhut (2018) and Hato (2017) in Hong Kong is about HK\$4.60 billion (~ US\$ 590 million) and HK\$1.21 billion (~ US\$ 155 million), respectively (Choy et al. 2020). Meanwhile, the impacts of climate change on TCs have the potential to significantly alter their influence on future coastal residents (Knutson et al. 2010, Tsuboki et al. 2015, Tran et al. 2022). The global warming trend is expected to continue or even worsen in the rest of the 21st century (Knutson et al. 2010). A recent comprehensive assessment by Knutson et al (2020) shows that a 2°C anthropogenic global warming is projected to impact TC activity as follows: 1) Medium-to-high confidence in the increased precipitation rates by

around + 14%, or close to the rate of tropical water vapor increase with warming; 2) Medium-to-high confidence in the + 5% stronger lifetime maximum surface wind speeds; 3) Medium-to-high confidence in a + 13% increase of the proportion of TCs that reach very intense (category 4–5) levels; and 4) The most confident TC-related projection is that sea level rise accompanying the warming will lead to higher storm inundation levels, assuming all other factors are unchanged (Knutson et al. 2020). However, research conclusions are more mixed, and confidence levels are lower for the basin-scale or regional projections (Knutson et al. 2020, Bloemendaal et al. 2022). Due to the limitation in spatial resolution, Global Climate Model (GCM) studies also introduce large biases when reproducing TC activities on a regional scale (Bloemendaal et al. 2022). These factors fall far short of satisfying the demand to guide regional climate change adaptation and resilience.

On a regional scale, air-sea interaction plays a crucial role in the development of TCs. As noted by Emanuel (1986), the ocean surface enthalpy fluxes transferred to the atmosphere are the main energy sources of TCs. The Coupled Model Intercomparison Project Phase 6 (CMIP6) model results indicate that in the future, there will be a warmer and fresher surface ocean. This implies an increased thermal stratification in a warming climate, which in turn will feedback on the TC development (Huang et al. 2015, Balaguru et al. 2016). Additionally, studies have shown that at extremely high surface wind speeds (30 m/s or higher), the roughness length, determined by the sea state, tends to plateau. This can maintain or even enhance the inner-core intensity of the TC (Moon et al. 2004, Chen et al. 2013). Numerical studies incorporating such effects can construct more realistic TC structures than atmosphere-only or even atmosphere–ocean coupled models (Davis et al. 2008, Chen et al. 2013, Wu et al. 2019). Consequently, operational centers such as the European Centre for Medium Range Weather Forecasts (ECMWF) are now using atmosphere-wave-ocean (AWO) coupled models to generate routine global products for better performance in TC forecasts (Mogensen et al. 2017, Magnusson et al. 2019). Incorporating a dynamically evolving 3-dimensional ocean model and a wave model at convection-permitting scales (i.e., 4 km or finer; see Zhang et al. 2011) is crucial to better capture the TC-related coastal disasters on a regional scale. By generating crucial products related to coastal hazards across the atmosphere (wind and rainfall), sea wave (significant wave height), and ocean (storm surge level) from the synergistic framework, valuable supporting evidence can be provided to guide regional adaptation and resilience against TCs in a changing climate.

The objective of this study is to investigate the impact of future TC-related coastal disasters on the PRD region in a changing climate, using a sophisticated AWO coupled model. The PRD region is home to numerous large populations and is a pivot of manufacturing, finance, and marine industries such as shipping and aquaculture in China. To achieve this objective, we examine three intense landfalling TCs since 2010 in “parallel digital worlds”: a present-day world and a warming future world. Specifically, we conduct simulations using (a) present-day reanalysis data and (b) the same TCs occurring in a pseudo-global warming (PGW) scenario projected for the end of the 21st century. Conventional PGW experiments have been extensively used in atmospheric-only regional models such as the WRF (Chen et al. 2020, Jyoteeshkumar et al. 2021, Tran et al. 2022). To our knowledge, this study is the first to implement PGW in an AWO fully coupled system over the PRD region, achieving such high horizontal resolutions (1-km

atmosphere and 500-m ocean and sea wave). The perturbed warming initial and boundary conditions are derived from both atmosphere and ocean GCMs projected by CMIP6 and enforced in both the atmosphere and the ocean components of the fully coupled system. The results of this study will provide valuable insights into the potential impacts of future TC-related coastal disasters on the PRD region and guide regional adaptation and resilience against such disasters in the changing climate.

Modeling system and experimental design

2.1 The Coupled Ocean–Atmosphere–Wave–Sediment Transport (COAWST) modeling system

The COAWST system serves as the fundamental framework for this study. It is an agglomeration of open-source modeling components tailored to investigate coupled processes of the atmosphere, ocean, and waves in coastal regions. Since its release by the United States Geological Survey in 2010, it has been widely used in various studies (Warner et al., 2010). COAWST has been applied to examine several Atlantic TCs that caused considerable damage in North America, such as Ivan (2004), Ida (2009), and Sandy (2012) (Olabarrieta et al. 2012, Zambon et al. 2014a, Zambon et al. 2014b). In this study, we use COAWST v3.6, which comprises the following modules: (1) an atmospheric component named Weather Research and Forecasting Model (WRF v4.1.2); (2) a Regional Ocean Modeling System (ROMS) v3.7 as an oceanic component; (3) a SWAN v41.31 as a sea wave component; and (4) a Model Coupling Toolkit (MCT) v2.6.0 as a coupler.

In previous work by Li et al (2022), the COAWST has been customized and tuned extensively to suit local weather and climate studies in the PRD region. It was used to investigate the impact of sea wave-wind interaction on TC development, including typhoon tracks and intensities. The current system builds upon this framework and is organized into a hierarchical architecture with two tiers, each tailored to simulate dominant physical processes at corresponding spatial scales (see Fig. 1). Tier 1 is designed for open sea scale modeling. The WRF model is configured with a horizontal resolution of 9 km × 9 km in its outermost domain (WRF D01). The ROMS and SWAN models (ROMS + SWAN D01) are nested within WRF D01, with an ocean eddy-resolving resolution of 2.2 km × 2.2 km. The intermediate domain for WRF (WRF D02) is embedded in ROMS + SWAN D01 at sea, with a convection-permitting resolution of 3 km × 3 km. Tier 2 is designed to provide high spatial resolution for modeling the PRD coastal region. The innermost WRF domain (WRF D03) has a resolution of 1 km × 1 km and covers the entire PRD region. The innermost ROMS + SWAN domain (ROMS + SWAN D02) has a resolution of 500 m × 500 m and covers the Pearl River estuary and the nearshore sea.

The configurations for each of the three component models follow Li et al. (2022), with minor modifications made for computational efficiency. These modifications include a smaller mesh size in WRF D01/02 and ROMS + SWAN D01. In addition, the number of vertical layers in the WRF model is reduced to 39 layers, but the number of vertical layers within 1,500 m above the surface is increased to 19 for improved accuracy in representing physical processes and structures in the planetary boundary layer.

For air-wave interaction, we implemented Lin and Sheng (2020) scheme, which is embedded in the Mellor-Yamada-Nakanishi-Niino (MYNN; Nakanishi and Niino 2004) planetary boundary layer scheme and associated surface layer schemes. Detailed configurations are summarized in Table S1. Tide information was obtained from the Oregon State University Tidal Prediction Software (OTPS; Egbert and Erofeeva 2002), which provides data on eight primary harmonic constituents (M2, S2, N2, K2, K1, O1, P1, Q1).

2.2 Experimental design

In this study, we selected three intense landfalling TCs - Mangkhut (2018), Hato (2017), and Vicente (2012) - which caused significant impacts on the PRD coastal areas. These selected TCs were then simulated using the COAWST framework. Two groups of experiments were conducted: present-day control (CTRL) experiments and pseudo-global warming (PGW) experiments. The CTRL experiments aimed to reproduce the selected TCs and related coastal disasters with high fidelity, including rainfall, wind, storm surges, and storm waves. The PGW experiments aimed to simulate the same storms occurring in a global warming scenario projected for the end of the 21st century.

We utilized the high-resolution version of the Max Planck Institute Earth System Model (MPI-ESM-1-2-HR) from CMIP6 datasets to extract PGW signals (Gutjahr et al. 2019). Thermo-variables, including air temperature, humidity, sea water temperature, and sea water salinity, were extracted from 2090–2099 in the Shared Socioeconomic Pathways 5-8.5 (SSP5-8.5) scenario and 2005–2014 in the historical simulation. The differences between the two epochs were then added to the initial and boundary conditions of the WRF and ROMS models. Figure S2 and figure S3 show the changes in July-August-September 2090s for the SSP5-8.5 scenario, including a projected 2.4°C warming of Sea Surface Temperature (SST) in the outermost domain and a 2.6°C warming of the 25–50 m subsurface ocean. Specific humidity near the surface level is expected to increase by 3.0–4.0 g/kg, and the surface air temperature will increase by 3.2°C, with more than 6.0°C warming in the upper level (near 250 hPa, see figure S3). We compared the results with the multi-model ensemble mean and a previous study by Chen et al. (2020) based on CMIP5 output and found similar changes in variable magnitudes and large-scale patterns. To our knowledge, this is the first time the PGW method has been applied in a regional AWO coupled model to study future TC activities.

Results

3.1 Simulation basics and model evaluation

We begin by comparing the tracks and intensities of the selected TCs in both the CTRL and PGW experiments. The successful reproduction of TC evolutions in the CTRL experiments provides a higher level of confidence for future projections. As depicted in Figs. 2a–c, the COAWST model performed quite well in capturing the tracks of all selected TCs, including the stable steering flow caused northwest-southeast tracks of Mangkhut (2018) and Hato (2017) from the western Philippine waters to the southern China coast. Notably, the model effectively simulated the subtle but essential episode of Vicente (2012),

where it slowed down and remained stagnant over the northern South China Sea on July 22, 2012, as the subtropical ridge northeast of the storm suddenly weakened (Chen et al. 2017). While the track for TC Vicente (2012) exhibited an evident southward track shift compared with the observation and future run near 111°E, 22°N. This southward track deflection is a typical behavior regarding the terrain effect over the western Guangdong Province, similar effect in Taiwan has been well archived by Wu et al. (2015).

Figures 2d–f and 2g–i display the central minimum sea level pressures (SLPs) and maximum 10-m wind speeds, respectively. It is noteworthy that the COAWST underestimates the central SLPs in all cases, which is a known bias of the WRF model, even in cloud-resolving resolution without vortex initialization (Wu et al. 2006, Tong et al. 2018, Chang et al. 2020, Chen et al. 2020). To address this issue, we tested the insertion of the Rankine vortex to the initial condition based on the real TC intensity and location through the WRF TC “bogus” scheme in Hato (2017). However, this technique resulted in a remarkable overestimation of surface wind and unreasonably high storm surge levels when compared with in-situ observations (discussed later). As a trade-off, experiments were conducted without “bogus” TC to better simulate more direct coastal disaster indicators, despite the underestimation of central SLPs.

We compared the changes in tracks and intensities between the PGW and CTRL experiments. To ensure the constancy of ensuing analysis, we used large-scale spectral nudging of steering wind with appropriate relaxation coefficients, and all TCs in the PGW experiments kept similar tracks to those in CTRL. Additionally, since spectral nudging tends to suppress the TC intensity (Moon et al. 2018), we conducted experiments without nudging, and the results indicated that the tracks could deflect by hundreds of kilometers, although the minimum SLP deepened by around 5 hPa (Figure S4).

For intensity comparison between the PGW and CTRL, both Mangkhut (2018) and Hato (2017) exhibited a slight drop in the minimum SLP by 3–7 hPa, which is similar to recent studies on TCs impacting Southeast Asia (Chen et al. 2020, Jyoteeshkumar et al. 2021, Tran et al. 2022). However, for Vicente (2012), we found a sharp drop in the central SLP in the PGW experiment, which was 15 hPa lower than that in CTRL. The unusual stationary track over the northern South China Sea allowed Vicente (2012) to absorb excess energy from the warmer and stabler ocean in a warming future. In the CTRL simulation, the mean SST beneath the stationary location of Vicente (2012) dropped from around 29.3°C to 27.5°C, whereas in PGW, it dropped from around 32.1°C to 30.0°C. Even after strong upper-ocean mixing by Vicente (2012), the SST is still warmer than the initial SST over that location in CTRL (Figure not shown). Regarding the maximum surface wind speed, the time series show similar evolution, but intense peak wind strengthening can be found in the PGW. Mangkhut (2018) and Hato (2017) exhibited a peak surface wind speed that was approximately 4 m/s (~ 10%) higher, which is consistent with the results from Chen et al. (2020) study on three different TCs affecting the PRD in the far future (2075–2099). Particularly, Vicente (2012) even attained nearly 10 m/s (~ 30%) increase in maximum 10-meter wind speed due to further intensification.

In addition to evaluating performance in tracks and intensities, evaluating the performance of the COAWST using in-situ station-based observations are also important, as major coastal disasters caused

by TCs are fierce wind, torrential rainstorms, and formidable storm surges and waves. Consequently, 10-m wind speed and accumulated rainfall are compared with 2739 surface automatic weather stations in Guangdong province (Figure S5a). Quality control is implemented, and stations with accumulated rainfall less than 50 mm in each TC exposure are eliminated in rainfall evaluation. Table 1 shows that the model overestimates the wind speed by 1.2 m/s (+ 7.4%) with 5.7 m/s root mean square error (RMSE) during the TC exposure. For accumulated rainfall, the COAWST underestimated accumulated rainfall by 4.8 mm (-2.8%) across all qualified stations. While the RMSE is 70.6 mm, relatively small mean bias and large RMSE indicate the model performs okay in reproducing the mean rainfall amount but poorly captures the fine-scale spatial distribution. We then compared storm surge levels using the Hong Kong Observatory tide gauges in Hong Kong (Fig. S4b). Tide-induced water level fluctuations relative to the Chart Datum were linearly combined with the pure storm surge level produced by COAWST to represent the total surge. Results indicate that the simulated surge level is overestimated by 0.13m (+ 5.5%) with RMSE 0.35m. The two metrics show that the model can reproduce the surge variability for the three cases with reasonable accuracy (order of 10 cm) in this region, similar to the magnitude compared with previous studies using various models (Wang et al. 2008, Yin et al. 2020, Chen et al. 2020). Following Li et al. (2022), significant wave height is compared with in-situ wave observations at four buoys (QF303, QF304, QF306, and QF307) located in the continental shelf sea in the northern South China Sea (see Figure S4c), within 100-km distances to the nearest coast. Due to limited data availability, the significant wave height is only evaluated for Mangkhut (2018), with - 0.56 m (-9.3%) underestimation in mean bias and RMSE 1.12 m. Still, it shows the ability of the wave model to produce reliable wave height, given that the wind can be reasonably simulated by the atmospheric model.

Table 1
Station observations in comparison with model simulations

	Mean bias	Relative bias	Root mean square error
10-m wind speed (m/s)	+ 1.2	+ 7.4%	5.7
Accumulated rainfall (mm)	-4.8	-2.8%	70.6
Storm surge level (m)	+ 0.13	+ 5.5%	0.35
Significant wave height (m)	-0.56	-9.3%	1.12

3.2 Changes in wind and precipitation

Severe wind can cause dramatic damage in coastal regions, especially for metropolises such as Shenzhen and Hong Kong in the PRD region. During Mangkhut (2018), the collapse of trees caused extensive road blockage, paralyzing land transportation. Broken windows and falling debris due to building damages seriously threaten the safety of residents (Choy et al. 2020). Figure 3 estimates the grid-wise maximum 10-m wind speed change using the PGW experiment minus the CTRL. Negative values are masked out for clarity.

All three cases result in an increase in the 10-m maximum wind speed in the PGW experiments for the areas exposed by the TC circulation, especially for the coastal area where it is exposed to the TC right-of-track. Please note that the difference in 10-m wind are probably coming from the variation (drift) of TC's center in the two experiments rather than the change in intensity. To eliminate this effect, quantitative analysis based on the distance to TC's center has been implemented. For example, the maximum 10-m wind speed within 50–200-km right to the TC center increases by 4.3 m/s (22%). Tran et al. (2022) attributed the increase in the TC right-of-track surface maximum wind speed to the faster transition speed of the TCs. While our study's three cases cannot definitively conclude that TCs are moving faster, the stronger intensity of these storms will certainly contribute to higher wind speed exposure for vulnerable coastal regions. In the case of Vicente (2012), which experienced the largest intensity increment in the PGW experiment, large areas of increased wind speed were found within the coverage of the TC's circulation. On average, the maximum 10-m wind speed within 50–200 km to the right of the TC center increased by 6.9 m/s (39%). In a warming future, special attention should be paid to TCs with stationary tracks, like Vicente (2012), as they are likely to experience abrupt and acute rapid intensification near the shore, resulting in much greater wind impacts on coastal areas (Fig. 3c).

TCs often bring torrential rainfall, which can cause severe flooding and landslides, adding to the list of coastal disasters associated with these storms. The resulting damage to infrastructure, property, and loss of life can be catastrophic, particularly in low-lying or densely populated areas. Figure 4 shows the grid-wise histogram of accumulated rainfall (mm) and hourly rain rate within a radius of 500 km of the TC center over the lifetime. The blue solid curve represents the CTRL experiment, and the red dashed curve represents the PGW experiment. A robust accumulated rainfall increase was observed in all three cases, with an average of 96.9 mm in CTRL and 107.9 mm in PGW, representing an 11.7% increase. Previous studies have shown that the global TC precipitation increases by slightly more than 7% per 1°C of tropical SST warming (the Clausius–Clapeyron relation) in multiple climate model projections (Knutson et al. 2020). Given that the domain-averaged additional SST perturbation is about 2.4°C, an 11.7% increase in accumulated rainfall is slightly lower than the Clausius–Clapeyron relation. However, the extreme tails exhibit a slightly super-Clausius–Clapeyron relation, suggesting that special attention should be paid to extreme rainfall events. As shown in Fig. 4a–c, the PGW experiment significantly increased the percentage of accumulated rainfall by more than 200 mm in the three cases, from 11.0–13.9% (+ 26.4%). The 99th and the 99.9th percentile of accumulated rainfall threshold increased, from 405 mm to 475 mm (+ 17.3%), and from 619 mm to 735 mm (+ 18.6%), respectively. For the hourly rain rate (≥ 0.1 mm/h), the 99th and the 99.9th percentile of hourly rain rate increased from 40.9 mm/h to 45.3 mm/h (+ 10.6%), and from 82.2 mm/h to 85.9 mm/h (+ 4.5%), respectively (Fig. 4d–f).

3.3 Sea waves and storm surges

TCs can cause devastating storm surges, which can be further exacerbated by spring tides, leading to catastrophic consequences such as flooding in low-lying areas, infrastructure damage, and loss of life, particularly in areas with poor drainage or inadequate flood protection. Local coastline geometry can also enhance flooding (Lowe et al. 2005, Wang et al. 2008, Wu et al. 2019, Lin et al. 2019). Wave-surge and

wave-current interactions are important processes during storm surges and can be resolved by coupling a 3-dimensional ocean model and a spectral sea wave model, such as COAWST (Olabarrieta et al. 2011, Benetazzo et al. 2013). Grid-level maximum significant wave height and storm surge height difference using PGW minus CTRL in ROMS + SWAN D02 are shown in Fig. 5. The changes in maximum significant wave height exhibit a complex pattern due to sensitivity to TC tracks (Fig. 5a/c/e). We found that, by masking out the ocean grid approximating the shoreline (see Figure S5), the maximum significant wave height at the ocean is lifted by 57 cm (+ 13.8%) on average. Notably, there is a large difference between Hato (2017) and Vicente (2012). In the PGW experiment, the surface wind speed on the left-hand side of the TC does not increase for Hato (2017), limiting wave generation. In contrast, more than a 200 cm wave height increase is observed at the open sea near the TC eyewall and along the coastline for Vicente (2012). Storm surge exhibits a relatively uniform increment pattern (Fig. 5b/d/f). On average, maximum pure surge levels are lifted by 30–80 cm over the open sea but increase much higher along the coastline, especially for narrowing estuaries where the maximum surge level can be lifted by up to 200 cm.

To better illustrate the effect on coastal regions, averaged changes for three cases on the oceanic coastal grids (see Figure S5) are shown in Fig. 5g–h. More than a 200 cm increase in significant wave height is observed over the offshore islands facing the open ocean, while the mainland coastline typically faced a 40–80 cm increase. The lee side of the islands generally did not face significant wave height increases more than 60 cm, and for most inner riverbanks, only a lower than 20 cm wave height increase can be found. Conversely, storm surge level is sensitive to coastline geometry (Fig. 5h), with the inner riverbanks facing more than a 60 cm increase in surge level. Most coastlines would face a 40–60 cm increase in storm surge, while only the sheltered Hong Kong central waters evaded the large surge level changes, with only a 20–40 cm additional water elevation. According to multi-model mean results from CMIP6, compared to the present-day climatology (1995–2014), global mean sea level rise will be 0.65 m at the end of the 21st century (2081–2100) in SSP5-8.5 (Hermans et al. 2021). In the context of the 2090s, a combination of mean sea level rise, storm surge, and wave height can reach more than a 300 cm increase in total water level at certain hot-spot coastlines, without considering the superposition of spring tides.

Conclusions and discussion

The PGW experiments, carried out by a novel AWO coupled model, mimic the thermodynamic conditions expected in the 2090s. The results suggest that changes in intense tropical cyclones (TCs) could have a significant impact on the PRD region, home to large populations, and the pivot of manufacturing, finance, and marine industries in China. Several coastal disaster indicators, including surface maximum wind speed, accumulated rainfall, hourly rain rate, storm surge height, and storm wave height, become more severe in the PGW experiments as the intensity of the selected TC cases increases. Our study highlights the particular concern of typhoons like Vicente (2012), which have stationary tracks and remain in warm waters for a long time. In a warming future, the warmer and stabler surface ocean, even after a long TC-induced "cold wake", which has an important negative feedback on TC intensity (Bender and Ginis 2000, Knutson et al. 2001), cannot weaken these types of TCs. They tend to experience abrupt and acute rapid intensification nearshore, resulting in a much shorter response time and greater impacts on coastal areas.

Our analysis focused on the extreme values in the wind speed distribution, and we found that the maximum 10-m wind speed within 50–200 km to the right of the TC center increased by 4.3 m/s (or 22%). For Vicente (2012), the increase was even greater at 6.9 m/s (or 39%). The increase in the TC right-of-track surface maximum wind speed may be attributed to the faster transition speed of the TCs, while the stronger intensity of these TCs tends to bring wind impacts further inland (Tran et al. 2022). Regarding the rainfall impact, we observed an average 11.7% increase in accumulated rainfall, corresponding to a slightly less than 7% per 1°C increase relative to tropical SST warming (the Clausius-Clapeyron relation). It is noteworthy that the percentage of accumulated rainfall by more than 200 mm will increase by 26.4%, and the 99th and 99.9th percentile of accumulated rainfall threshold will increase by +17.3% and +18.6%, respectively. The greater than 7% per 1°C increase of the right tail of the rainfall distribution indicates much more severe extreme precipitation caused by TCs, significantly increasing the risks of coastal landslides and flooding in a warming future.

Previous studies have shown that, assuming all other factors are unchanged, the most confident TC-related projection is that sea level rise accompanying the warming will lead to higher storm inundation levels (Knutson et al. 2020). In this study, we went beyond previous research by considering the surface wave component and its coupling with the 3-dimensional ocean and atmosphere. Simulation results show that even without considering the mean sea level rise and spring tides, stronger TC intensity in a warming climate can already push more than 100 cm of additional water level to most PRD coastlines by combining surge level and wave height changes. Given the significant uncertainties in mean sea level rise, especially for the mass loss in Greenland and Antarctic ice sheets (Hermans et al. 2021), from a risk management perspective, we suggest a stress test considering a total water level increase of more than 300 cm in the PRD region due to storm surge in the context of the 2090s, even without considering the overlap with spring tides. Such an approach would help to ensure that the PRD coastal areas and their populations are better prepared for future climate risks and can adapt to the potential impacts of TCs on coastal flooding.

It is important to note that our current study has several limitations. We have only examined three intense landfalling TCs since 2010s. The small sampling size would cause potential bias in future projections. Further studies, especially with a much larger sample size, are needed to confirm the current findings and explore other potential impacts of future changes in intense TCs on the PRD coastal regions. Meanwhile, it is important to acknowledge the limitations of our approach in studying the storm surge impact, as we did not use an inundation model to estimate the extent and depth of coastal flooding during storm surge events. This limitation may have restricted our ability to fully quantify the potential impacts of climate change on storm surges in the PRD region. Many other important parameters, e.g. the potential shift of the TC tracks in the warming climate and potential rapid intensification or rapid weakening of TCs over the study region are needed to be investigated by ensemble simulation technique. Ensemble technique also support robust analysis based on impact indices such as the power dissipation index (PDI, Emanuel 2005) and cyclone damage potential (CDP, Holland et al. 2019), which can be further incorporated to study the TC changes.

Declarations

Funding We appreciate the assistance of the Hong Kong Observatory (HKO) and Environmental Central Facility (HKUST), which provided the meteorological and model input data. This work is supported by grants from the Research Grants Council of the Hong Kong Special Administrative Region, China (Project No. AoE/E-603/18 and T31-603/21-N), the Environment and Conservation Fund (2022-02), the CORE Project 2022/23, and the CORE is a joint research center for ocean research between QNLM and HKUST.

Financial and non-financial interests

The authors have no relevant financial or non-financial interests to disclose.

References

1. Balaguru, K., Foltz, G.R., Leung, L.R. and Emanuel, K.A., 2016. Global warming-induced upper-ocean freshening and the intensification of super typhoons. *Nature Communications*, 7(1), p.13670.
2. Bender, M.A. and Ginis, I., 2000. Real-case simulations of hurricane–ocean interaction using a high-resolution coupled model: Effects on hurricane intensity. *Monthly Weather Review*, 128(4), pp.917-946.
3. Benetazzo, A., Carniel, S., Sclavo, M. and Bergamasco, A., 2013. Wave–current interaction: Effect on the wave field in a semi-enclosed basin. *Ocean Modelling*, 70, pp.152-165.
4. Bloemendaal, N., de Moel, H., Martinez, A.B., Muis, S., Haigh, I.D., van der Wiel, K., Haarsma, R.J., Ward, P.J., Roberts, M.J., Dullaart, J.C. and Aerts, J.C., 2022. A globally consistent local-scale assessment of future tropical cyclone risk. *Science Advances*, 8(17), p.eabm8438.
5. Chan JCL (2008) Decadal variations of intense typhoon occurrence in the western North Pacific. *Proc R Soc Lond A* 464:249–272. doi:<https://doi.org/10.1098/rspa.2007.0183>
6. Chang, Y.P., Yang, S.C., Lin, K.J., Lien, G.Y. and Wu, C.M., 2020. Impact of tropical cyclone initialization on its convection development and intensity: A case study of Typhoon Megi (2010). *Journal of the Atmospheric Sciences*, 77(2), pp.443-464.
7. Chen, J., Wang, Z., Tam, C.Y., Lau, N.C., Lau, D.S.D. and Mok, H.Y., 2020. Impacts of climate change on tropical cyclones and induced storm surges in the Pearl River Delta region using pseudo-global-warming method. *Scientific Reports*, 10(1), pp.1-10.
8. Chen, S. S., Zhao, W., Donelan, M. A., & Tolman, H. L. 2013. Directional wind-wave coupling in fully coupled atmosphere-wave-ocean models: Results from CBLAST-Hurricane. *Journal of the Atmospheric Sciences*, 70(10), 3198–3215.
9. Chen, X., Wang, Y., Zhao, K. and Wu, D., 2017. A numerical study on rapid intensification of Typhoon Vicente (2012) in the South China Sea. Part I: Verification of simulation, storm-scale evolution, and environmental contribution. *Monthly Weather Review*, 145(3), pp.877-898.
10. Choy, C.W., of Insurers, T.H.K.F., Wu, M.C. and Lee, T.C., 2020. Assessment of the damages and direct economic loss in Hong Kong due to Super Typhoon Mangkhut in 2018. *Tropical Cyclone Research*

and Review, 9(4), pp.193-205.

11. Chu, J.E., Lee, S.S., Timmermann, A., Wengel, C., Stuecker, M.F. and Yamaguchi, R., 2020. Reduced tropical cyclone densities and ocean effects due to anthropogenic greenhouse warming. *Science Advances*, 6(51), p.eabd5109.
12. Cummings, J.A. and Smedstad, O.M., 2013. Variational data assimilation for the global ocean. In *Data Assimilation for Atmospheric, Oceanic and Hydrologic Applications (Vol. II)* (pp. 303-343). Springer, Berlin, Heidelberg.
13. Egbert, G.D. and Erofeeva, S.Y., 2002. Efficient inverse modeling of barotropic ocean tides. *Journal of Atmospheric and Oceanic Technology*, 19(2), pp.183-204.
14. Emanuel, K.A., 1986. An air-sea interaction theory for tropical cyclones. Part I: Steady-state maintenance. *Journal of Atmospheric Sciences*, 43(6), pp.585-605.
15. Emanuel, K. A., 2005: Increasing destructiveness of tropical cyclones over the past 30 years. *Nature*, 436, 686–688. <https://doi.org/10.1038/nature03906>
16. Gutjahr, O., Putrasahan, D., Lohmann, K., Jungclaus, J.H., von Storch, J.S., Brüggemann, N., Haak, H. and Stössel, A., 2019. Max Planck Institute Earth System Model (MPI-ESM1. 2) for the high-resolution model intercomparison project (HighResMIP). *Geoscientific Model Development*, 12(7), pp.3241-3281.
17. Hermans, T.H., Gregory, J.M., Palmer, M.D., Ringer, M.A., Katsman, C.A. and Slangen, A.B., 2021. Projecting global mean sea-level change using CMIP6 models. *Geophysical Research Letters*, 48(5), p.e2020GL092064.
18. Holland, G.J., Done, J.M., Douglas, R., Saville, G.R. and Ge, M., 2019. Global tropical cyclone damage potential. *Hurricane risk*, pp.23-42.
19. Huang, P., Lin, I.I., Chou, C. and Huang, R.H., 2015. Change in ocean subsurface environment to suppress tropical cyclone intensification under global warming. *Nature Communications*, 6(1), p.7188.
20. Jyoteeshkumar Reddy, P., Sriram, D., Gunthe, S.S. and Balaji, C., 2021. Impact of climate change on intense Bay of Bengal tropical cyclones of the post-monsoon season: a pseudo global warming approach. *Climate Dynamics*, 56, pp.2855-2879.
21. Knutson, T., Camargo, S.J., Chan, J.C., Emanuel, K., Ho, C.H., Kossin, J., Mohapatra, M., Satoh, M., Sugi, M., Walsh, K. and Wu, L., 2019. Tropical cyclones and climate change assessment: Part I: Detection and attribution. *Bulletin of the American Meteorological Society*, 100(10), pp.1987-2007.
22. Knutson, T., Camargo, S.J., Chan, J.C., Emanuel, K., Ho, C.H., Kossin, J., Mohapatra, M., Satoh, M., Sugi, M., Walsh, K. and Wu, L., 2020. Tropical cyclones and climate change assessment: Part II: Projected response to anthropogenic warming. *Bulletin of the American Meteorological Society*, 101(3), pp.E303-E322.
23. Knutson, T.R., McBride, J.L., Chan, J., Emanuel, K., Holland, G., Landsea, C., Held, I., Kossin, J.P., Srivastava, A.K. and Sugi, M., 2010. Tropical cyclones and climate change. *Nature Geoscience*, 3(3), pp.157-163.

24. Knutson, T.R., Tuleya, R.E., Shen, W. and Ginis, I., 2001. Impact of CO₂-induced warming on hurricane intensities as simulated in a hurricane model with ocean coupling. *Journal of Climate*, 14(11), pp.2458-2468.
25. Li, Z., Tam, C.Y., Li, Y., Lau, N.C., Chen, J., Chan, S.T., Dickson Lau, D.S. and Huang, Y., 2022. How Does Air-Sea Wave Interaction Affect Tropical Cyclone Intensity? An Atmosphere-Wave-Ocean Coupled Model Study Based on Super Typhoon Mangkhut (2018). *Earth and Space Science*, 9(3), p.e2021EA002136.
26. Lin, N., Marsooli, R. and Colle, B.A., 2019. Storm surge return levels induced by mid-to-late-twenty-first-century extratropical cyclones in the Northeastern United States. *Climatic Change*, 154, pp.143-158.
27. Lin, S. and Sheng, J., 2020. Revisiting dependences of the drag coefficient at the sea surface on wind speed and sea state. *Continental Shelf Research*, 207, p.104188.
28. Liu, K.S. and Chan, J.C., 2020. Recent increase in extreme intensity of tropical cyclones making landfall in South China. *Climate Dynamics*, 55(5-6), pp.1059-1074.
29. Lowe, J.A. and Gregory, J.M., 2005. The effects of climate change on storm surges around the United Kingdom. *Philosophical Transactions of the Royal Society A: Mathematical, Physical and Engineering Sciences*, 363(1831), pp.1313-1328.
30. Magnusson, L., Bidlot, J. R., Bonavita, M., Brown, A. R., Browne, P. A., De Chiara, G., et al. (2019). ECMWF activities for improved hurricane forecasts. *Bulletin of the American Meteorological Society*, 100(3), 445–458.
31. Mogensen, K. S., Magnusson, L., & Bidlot, J. R. (2017). Tropical cyclone sensitivity to ocean coupling in the ECMWF coupled model. *Journal of Geophysical Research: Oceans*, 122, 4392–4412. <https://doi.org/10.1002/2017JC012753>
32. Moon, I. J., Ginis, I., & Hara, T. (2004). Effect of surface waves on Charnock coefficient under tropical cyclones. *Geophysical Research Letters*, 31, L20302. <https://doi.org/10.1029/2004GL020988>
33. Moon, J., Cha, D.H., Lee, M. and Kim, J., 2018. Impact of spectral nudging on real-time tropical cyclone forecast. *Journal of Geophysical Research: Atmospheres*, 123(22), pp.12-647.
34. Nakanishi, M. and Niino, H., 2004. An improved Mellor–Yamada level-3 model with condensation physics: Its design and verification. *Boundary-layer Meteorology*, 112, pp.1-31.
35. Olabarrieta, M., Warner, J.C. and Kumar, N., 2011. Wave-current interaction in Willapa Bay. *Journal of Geophysical Research: Oceans*, 116(C12).
36. Olabarrieta, M., Warner, J.C., Armstrong, B., Zambon, J.B. and He, R. (2012) Ocean– atmosphere dynamics during Hurricane Ida and Nor’Ida: An application of the coupled ocean–atmosphere– wave–sediment transport (COAWST) modeling system. *Ocean Modelling*, 43, pp.112-137.
37. Taylor, P. K., & Yelland, M. J. (2001). The dependence of sea surface roughness on the height and steepness of the waves. *Journal of Physical Oceanography*, 31(2), 572–590.
38. Tong, M., Sippel, J.A., Tallapragada, V., Liu, E., Kieu, C., Kwon, I.H., Wang, W., Liu, Q., Ling, Y. and Zhang, B., 2018. Impact of assimilating aircraft reconnaissance observations on tropical cyclone

- initialization and prediction using operational HWRF and GSI ensemble–variational hybrid data assimilation. *Monthly Weather Review*, 146(12), pp.4155-4177.
39. Tran, T.L., Ritchie, E.A., Perkins-Kirkpatrick, S.E., Bui, H. and Luong, T.M., 2022. Future Changes in Tropical Cyclone Exposure and Impacts in Southeast Asia From CMIP6 Pseudo-Global Warming Simulations. *Earth's Future*, 10(12), p.e2022EF003118.
 40. Tsuboki, K., Yoshioka, M.K., Shinoda, T., Kato, M., Kanada, S. and Kitoh, A., 2015. Future increase of supertyphoon intensity associated with climate change. *Geophysical Research Letters*, 42(2), pp.646-652.
 41. Wang, S., McGrath, R., Hanafin, J., Lynch, P., Semmler, T. and Nolan, P., 2008. The impact of climate change on storm surges over Irish waters. *Ocean Modelling*, 25(1-2), pp.83-94.
 42. Warner, J.C., Armstrong, B., He, R. and Zambon, J.B. (2010) Development of a coupled ocean–atmosphere–wave–sediment transport (COAWST) modeling system. *Ocean Modelling*, 35(3), pp.230-244.
 43. Wu, C.C., Chou, K.H., Wang, Y. and Kuo, Y.H., 2006. Tropical cyclone initialization and prediction based on four-dimensional variational data assimilation. *Journal of the Atmospheric Sciences*, 63(9), pp.2383-2395.
 44. Wu, C.C., Li, T.H. and Huang, Y.H., 2015. Influence of mesoscale topography on tropical cyclone tracks: Further examination of the channeling effect. *Journal of the Atmospheric Sciences*, 72(8), pp.3032-3050.
 45. Wu, J., Chen, Y., Liao, Z., Gao, X., Zhai, P. and Hu, Y., 2022. Increasing risk from landfalling tropical cyclone-heatwave compound events to coastal and inland China. *Environmental Research Letters*, 17(10), p.105007.
 46. Wu, L., Breivik, Ø. and Rutgersson, A., 2019. Ocean-wave-atmosphere interaction processes in a fully coupled modeling system. *Journal of Advances in Modeling Earth Systems*, 11(11), pp.3852-3874.
 47. Wu, W. and Leonard, M., 2019. Impact of ENSO on dependence between extreme rainfall and storm surge. *Environmental Research Letters*, 14(12), p.124043.
 48. Yin, K., Xu, S., Zhao, Q., Huang, W., Yang, K. and Guo, M., 2020. Effects of land cover change on atmospheric and storm surge modeling during typhoon event. *Ocean Engineering*, 199, p.106971.
 49. Zambon, J.B., He, R. and Warner, J.C. (2014a) Investigation of hurricane Ivan using the coupled ocean–atmosphere–wave–sediment transport (COAWST) model. *Ocean Dynamics*, 64(11), pp.1535-1554.
 50. Zambon, J.B., He, R. and Warner, J.C. (2014b) Tropical to extratropical: Marine environmental changes associated with Superstorm Sandy prior to its landfall. *Geophysical Research Letters*, 41(24), pp.8935-8943.
 51. Zhang, F., Weng, Y., Gamache, J. F., & Marks, F. D. (2011). Performance of convection-permitting hurricane initialization and prediction during 2008–2010 with ensemble data assimilation of inner-core airborne Doppler radar observations. *Geophysical Research Letters*, 38, L15810.

Figures

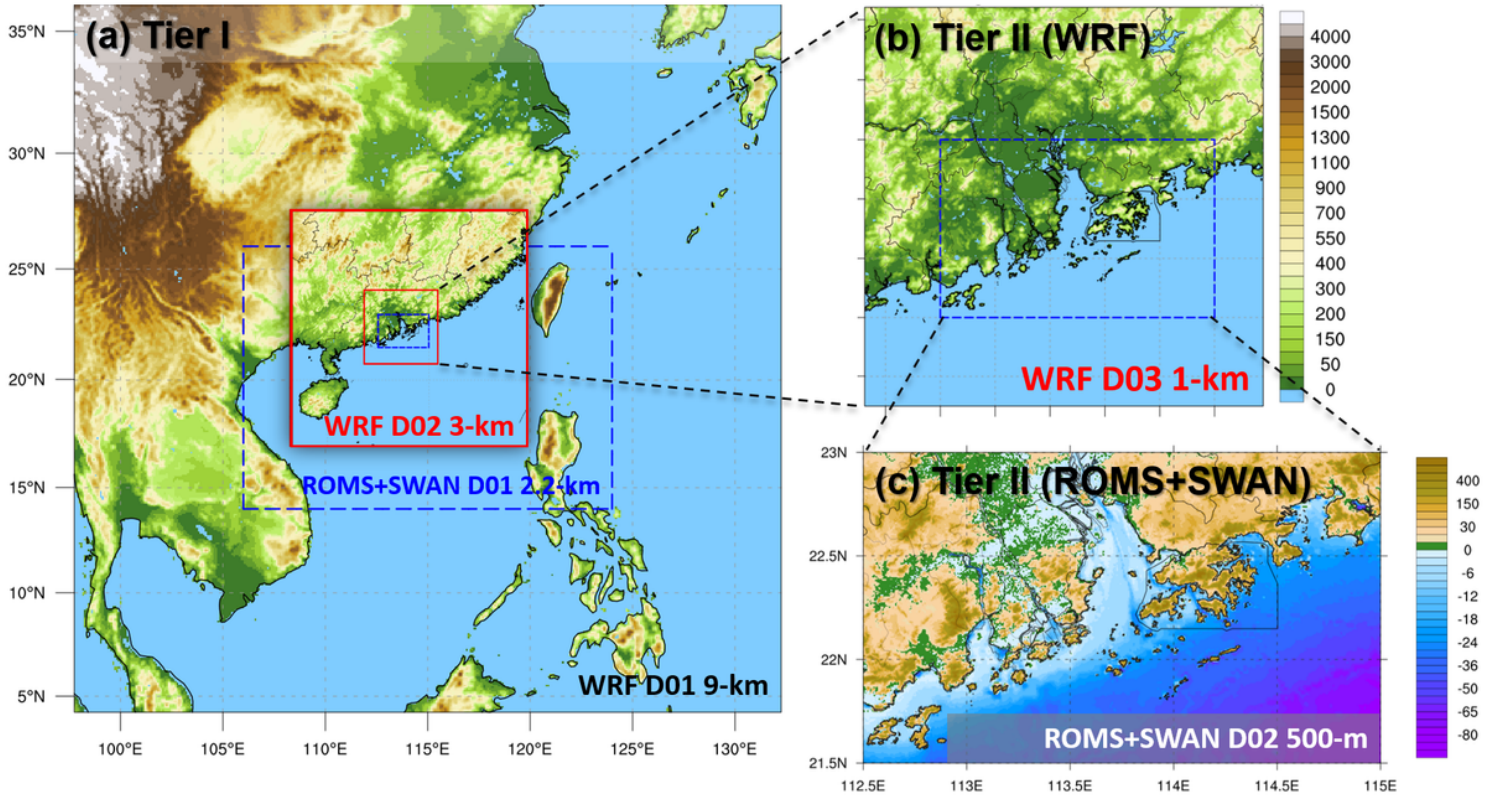


Figure 1

Domain configurations for the COAWST. (a) Tier 1 consists of the outermost 9-km WRF D01, with the intermediate 3-km WRF D02 enclosed in the red box. The blue dashed box represents the 2.2-km ROMS/SWAN D01. Tier 2 includes (b) the innermost WRF 1-km D02 that covers the entire PRD region, and (c) the innermost ROMS/SWAN D02, with a horizontal resolution of 500 m, covering the Pearl River estuary. The terrain height and bathymetry are shown using colored shading.

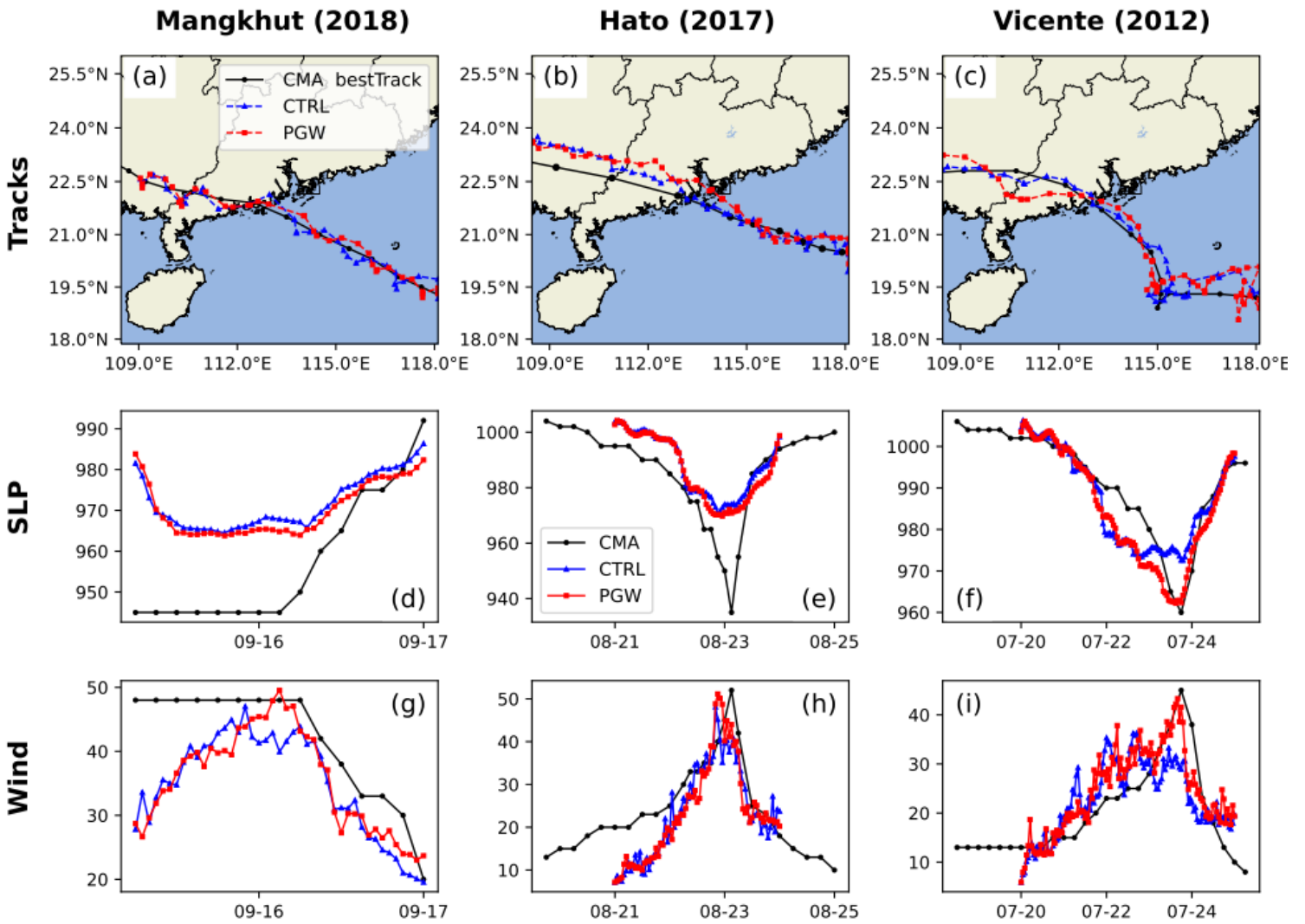


Figure 2

(a) Tracks of Mangkhut (2018) represented by the black solid curve for CMA best Track data, the blue dashed curve for the CTRL experiment, and the red dashed curve for the PGW experiment. (d) same as (a) but for the TC's minimum sea level pressure (hPa) evolution. (g) is same as (d) but for the maximum surface wind speed (m/s). (b) and (c), (e) and (f), and (h) and (i) show the same for Hato (2017) and Vicente (2012), respectively.

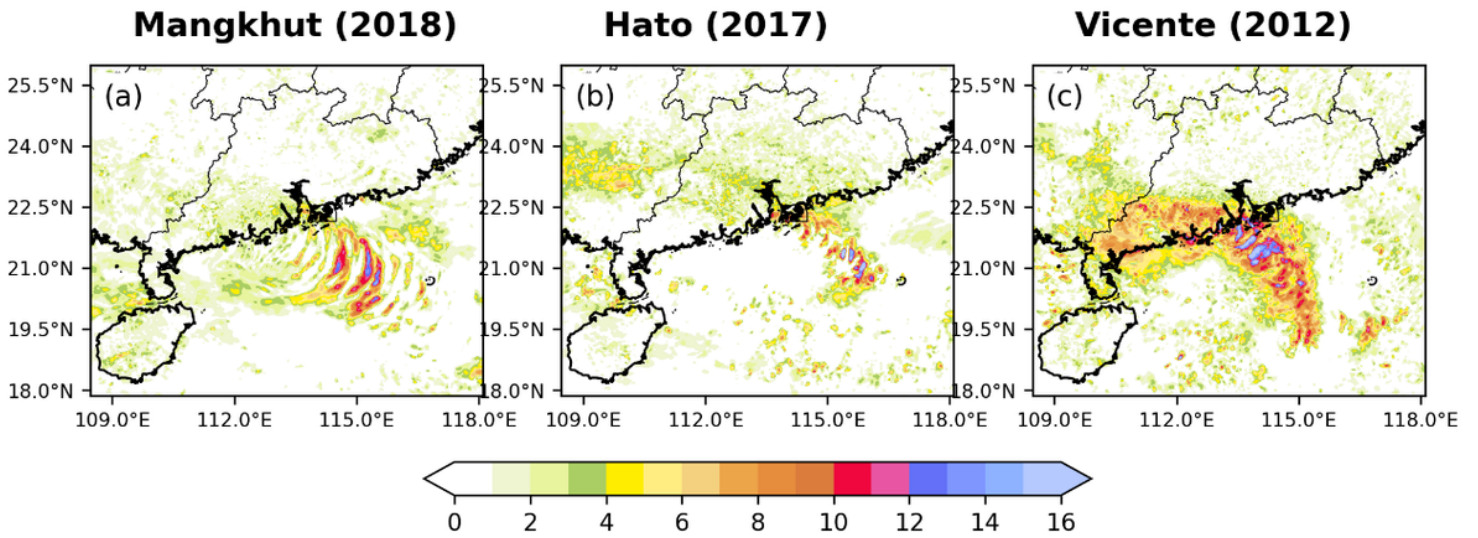


Figure 3

(a) Grid-wise maximum 10-m wind speed difference (in m/s) during the simulation period between PGW and CTRL simulations for Mangkhut (2018) in WRF d02. Negative values are masked out for clarity. (b–c) Same as (a), but for Hato (2017) and Vicente (2012), respectively.

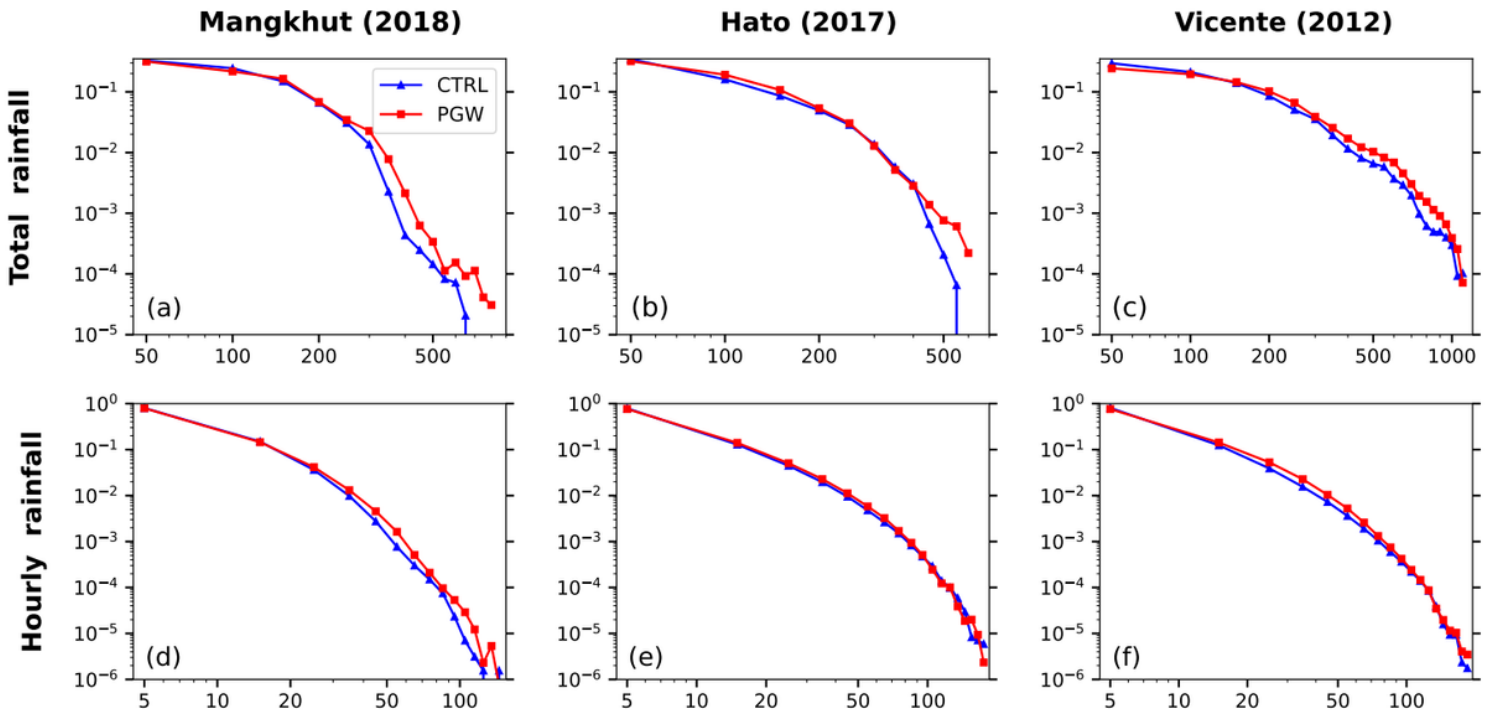


Figure 4

Histograms of accumulated rainfall (in mm) larger than 50 mm within a radius of 500 km from the TC center in WRF D02. The blue curve represents the CTRL experiment, while the red dashed curve represents the PGW experiment. (a) Mangkhut (2018), (b) Hato (2017), and (c) Vicente (2012) for accumulated

rainfall. (d) Mangkhut (2018), (e) Hato (2017), and (f) Vicente (2012) for hourly precipitation larger than 5 mm/hr.

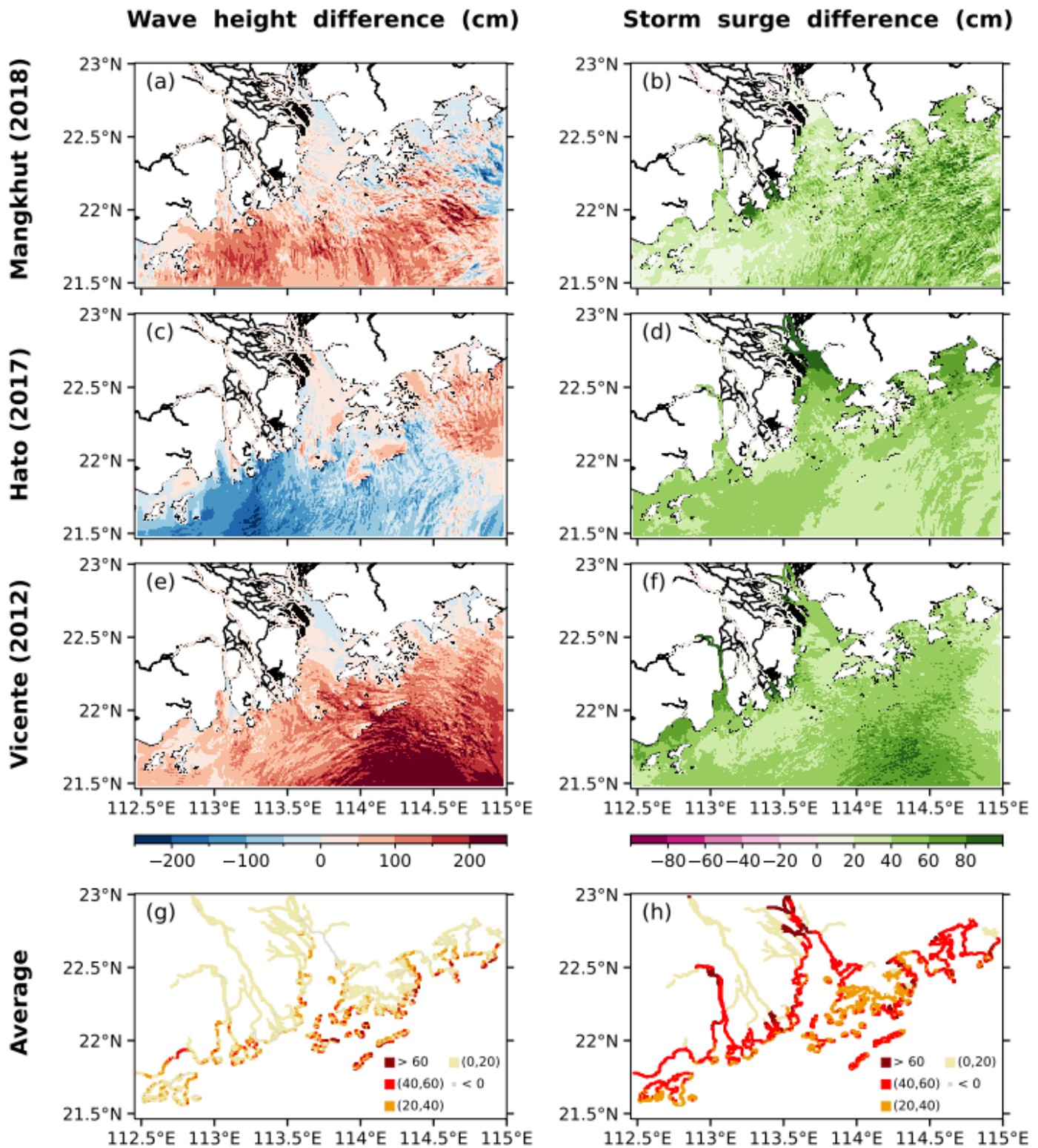


Figure 5

(a) Grid-level maximum significant wave height difference (cm) and (b) storm surge level difference (cm) using PGW minus CTRL for Mangkhut (2018) in ROMS+SWAN d02, (c-d) and (e-f), same as (a-b) but for

Hato (2017) and Vicente (2012), respectively. (g) and (h), three-case averaged coastal grid maximum significant wave height difference (cm) and storm surge level difference (cm).

Supplementary Files

This is a list of supplementary files associated with this preprint. Click to download.

- [SupplementaryInfo.docx](#)